Exciton ionization induced by intersubband absorption in nonpolar ZnO-ZnMgO quantum wells at room temperature

A. Jollivet,[1,*] P. Quach,[1] M. Tchernycheva,[1] R. Ferreira,[2] E. Di Russo,[3] L. Rigutti,[3] B. Vinter,[4] N. le Biavan,[4] D. Lefebvre,[4] M. Hugues,[4] J-M. Chauveau,[4] and F. H. Julien[1]

[1]*Centre de Nanosciences et de Nanotechnologies, CNRS, Université Paris-Saclay, 91120 Palaiseau, France*

[2]*Laboratoire de Physique de l'Ecole Normale Supérieure, ENS, Université PSL, CNRS, Sorbonne Université, Université de Paris, F-75005 Paris, France*

[3]*Normandie Université, UNIROUEN, INSA Rouen, CNRS, Groupe de Physique des Matériaux, 76000 Rouen, France*

[4]*Université Côte d'Azur, CNRS, CRHEA, rue Bernard Gregory, Sophia Antipolis, 06560 Valbonne, France*

(Received 30 January 2022; revised 25 April 2022; accepted 3 May 2022; published 26 May 2022)

We present a systematic investigation of intersubband transitions in nonintentionally doped *m*-plane ZnO/ZnMgO quantum wells (QWs). The investigation is performed using photoinduced absorption spectroscopy at room temperature under optical pumping by a UV laser to generate electron-hole pairs. All samples exhibit TM-polarized intersubbandlike absorption resonances. However, the peak transition energy is largely blueshifted (>100 meV) with expectations from electronic quantum confinement simulations. Based on calculations of the exciton binding energies, we attribute the photoinduced absorption at room temperature to the dissociation of hh_1-e_1 excitons towards free carriers in the e_2 state and not to hh_1-e_1 to hh_1-e_2 excitonic transitions induced by the intersubband absorption as previously stated by Olszakier *et al.* [Phys. Rev. Lett. **62**, 2997 (1989)]. This effect is a consequence of the huge binding energy of excitons in the ZnO material system, which is further enhanced in QWs due to the quantum confinement. This may pave the way for a better understanding of semiconductors' excitonic processes as well as for developing intersubband devices with a blueshifted operating range.

DOI: 10.1103/PhysRevB.105.195143

I. INTRODUCTION

Wide-gap semiconductors appear as promising materials in order to develop intersubband (ISB) devices in the whole infrared range. In particular, ZnO/ZnMgO heterostructures have recently attracted renewed interest for far-infrared ISB devices. ISB absorption has initially been observed at room temperature in wurtzite polar ZnO materials grown along the *c* axis [1,2]. In addition, it was predicted that the large energy (72 meV) of longitudinal optical (LO) phonons in ZnO provides room for THz quantum cascade lasers (QCLs) operating at record-high temperatures [3] much larger than that of the driving technology based on GaAs/AlGaAs THz QCLs [4]. Nonpolar ZnO/(Zn,Mg)O quantum wells (QWs) grown on *m*-plane ZnO substrates would be even better suited materials for quantum cascade devices, lasers, or detectors, because of the absence of internal electric fields which greatly simplifies their design. ISB absorption in *m*-plane *n*-doped ZnO/ZnMgO QWs has been recently observed at midinfrared wavelengths [5]. It was shown that the electron concentration in the ground state ($3-8\times10^{12}\,\mathrm{cm}^{-2}$) [6] leads to a significant blueshift of the ISB transitions with respect to the values calculated for an unpopulated QW due to the depolarization shift which is a manifestation of the screening of the incoming radiation by the ISB plasmons [7]. Such effect was also observed in early prototypes of nonpolar ZnO/ZnMgO quantum cascade detectors operating at short infrared wavelengths up to room temperature [8].

In order to get rid of the depolarization effect one should investigate bare ISB transitions in undoped QWs. One solution is to make use of the photoinduced absorption (PIA) spectroscopic technique [9,10]. The technique developed in the late 1980s involves a chopped interband excitation at a photon energy above the QW band gap to generate electron-hole pairs in their respective ground states and to probe the resulting infrared ISB absorption change using a lock-in amplifier. This differential technique, which allows probing absorption changes as low as $10^{-4}-10^{-6}$, is applicable to both undoped and doped QWs. The typical photogenerated electron concentration, which depends on the pump intensity, is in the range of $10^{9}-10^{10}\,\mathrm{cm}^{-2}$ [9,10], which is well below the exciton Mott transition and is too low to provide any significant contribution of many-body effects such as the depolarization shift. In addition, PIA does not require a reference sample since the reference is provided by the sample transmission without excitation. PIA has been successfully applied to various material systems such as GaAs/AlGaAs, SiGe/Si, and GaN/AlN QWs or InAs/GaAs quantum dots and InAs/AlInAs quantum dashes [9–14].

In the pioneering work of Olszakier *et al.* on GaAs/AlGaAs QWs at cryogenic temperatures down to 2 K, PIA was ascribed to excitonic transitions from hh_1-e_1 to hh_1-e_2 induced by the ISB absorption. However, no estimation of the hh_1-e_2 excitonic binding energy was provided [9]. Similar experiments performed on GaAs/AlGaAs QWs at

*Corresponding author: arnaud.jollivet@c2n.upsaclay.fr

room temperature did not reveal any excitonic effect because the binding energy of excitons is much lower than the thermal energy; i.e., the PIA only involves free carriers [10]. In turn, ZnO QWs appear as a model system to investigate the excitonic effects on photoinduced intersubband absorption at room temperature because of the huge binding energy of excitons in the ZnO material system (∼60 meV in bulk ZnO). At room temperature, photoexcited carriers in ZnO QWs are bound by Coulomb interaction and only excitonic interband transitions are present.

II. SAMPLE DESCRIPTION

In this paper, we have carried out a systematic investigation of ISB transitions in nonintentionally doped *m*-plane ZnO/ZnMgO QWs using PIA spectroscopy at room temperature. A series of samples with various well thicknesses and an Mg concentration in the barriers around 40% has been grown by molecular beam epitaxy (MBE). In addition to PIA, the samples have been characterized by photoluminescence, x-ray diffraction (XRD), transmission electron microscopy (TEM), and atom probe tomography (APT). All samples exhibit TM-polarized ISB-like photoinduced absorption. However, the peak PIA ISB transition energy is blueshifted by around $110 - 140$ meV with respect to the value predicted by electron quantum confinement simulations. These simulations were performed using NEXTNANO software [15] by solving the Schrödinger equation with a mass-effective model accounting for the uncertainty on the Mg content, QW thickness, and the actual value of the conduction band (CB) offset. The parameters used in NEXTNANO software are reported in the Supplemental Material [16] (also see Refs. [17–22]). This discrepancy can only be explained by excitonic effects. We have carried out extensive simulations of the hh_1-e_1 (X_1) and hh_1-e_2 (X_2) exciton binding energies following Ref. [23]. The comparison with the measurements of the calculated intersubband energy corrected by the exciton binding energies shows that the observed PIA transitions cannot be attributed to X_1 to X_2 excitonic transitions induced by the ISB absorption as previously stated by Olszakier *et al.* [9] and theoretically investigated by Sadeghi and Li [24]. In turn, good agreement with the experimental results is observed when accounting only for the X_1 exciton binding energy. We therefore claim that the photoinduced intersubband absorption in ZnO/ZnMgO QWs arises from the X_1 exciton ionization to free carriers in the e_2 state induced by the intersubband absorption. This effect is again a consequence of the huge binding energy of excitons in the ZnO material system [25] which is further enhanced in QWs due to the quantum confinement [26–28].

The investigated samples were grown on $10\times20\,\mathrm{mm}^2$ *m*-oriented ZnO substrates (Crystec) by MBE. The substrates were annealed at 1065 °C under an oxygen (O) atmosphere to reveal atomic steps. The atomic O was provided by a plasma cell operating at 420 W, and the O flow was set to 0.3 SCCM (standard cubic centimeter per minute). The substrate temperature was set to 420 °C. The Zn and O fluxes were adjusted to be close to stoichiometry to limit defect concentrations with a growth rate of 170 nm/h. The structures consisted of a 150 nm ZnO buffer layer followed by 15-period ZnO/ZnMgO QWs with a nominal Mg concentration of 40% and a barrier thickness of 15 nm. The whole structure is nonintentionally doped. The nominal well thickness of the seven investigated samples labeled A–G is 2.2, 2.6, 3.0, 3.2, 3.4, 3.7, and 4 nm, respectively.

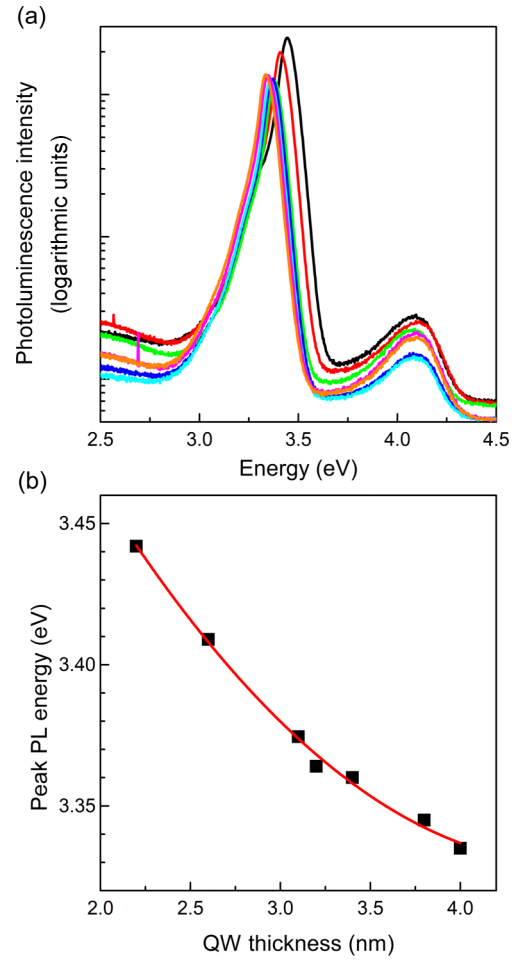

FIG. 1. (a) Photoluminescence spectra of the samples at room temperature. (b) The red dots are peak PL energy of the ZnO QWs versus the well thickness; the red curve corresponds to the simulated gap energy.

Figure 1(a) shows the photoluminescence (PL) spectra of the samples at room temperature. The peak at low (high) energy arises from the ZnO QWs (ZnMgO barrier). Figure 1(b) plots the QW peak PL energy versus the well thickness. As expected, the peak PL energy decreases with increasing well thicknesses. Based on the high-energy PL peak, the average Mg concentration is estimated to be in the range $39.1\% - 40\%$.

TEM and APT measurements performed on samples A and G confirm that the actual well thickness is within ±1 monolayer (ML, 0.23 nm) close to the nominal thickness. However, the analysis reveals a coherent corrugation within the multiple QWs with V grooves in the QW planes aligned along the *c* axis. Such morphology has already been observed in *m*-plane ZnO/ZnMgO QWs linked to the different adatom diffusion along the *c* axis and the *a* axis [29]. In addition,

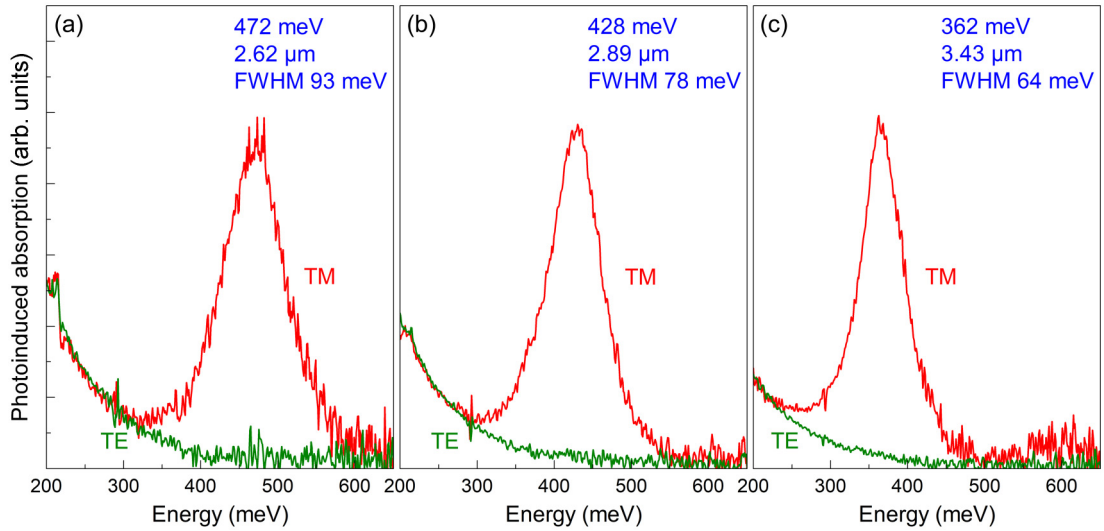

FIG. 2. PIA spectra of samples A (left), B (center), and C (right) at room temperature for TM- and TE-polarized light.

APT reveals that the Mg concentration in each individual QW varies by ±10% in absolute value with a maximum (minimum) value at the bottom (apex) of the V grooves [30]. The structural characterizations of these samples were performed with another set of samples with similar features; more details may be found in Ref. [30].

III. EXPERIMENTAL METHOD AND RESULTS

For PIA spectroscopic measurements, the samples were mechanically polished to form a multipass waveguide with two internal reflections and 45° angle facets. Interband excitation at 266 nm was provided by a Spectra-Physics Millennia visible laser frequency doubled with a WaveTrain. The UV light was mechanically chopped at 1 kHz and focused at normal incidence onto the sample surface with a spot size of 2 mm. A liquid nitrogen cooled HgCdTe detector was used to detect the infrared sample transmission change (ΔT) along with a lock-in amplifier. Figure 2 shows PIA spectra of samples A, B, and C for TM- and TE-polarized lights recorded with a Bruker Vertex 70 Fourier transform infrared spectrometer (FTIR) operated in a step-scan mode. The pump power was fixed at 100 mW. The differential absorption is divided by the transmission of the samples without UV illumination measured in the rapid-scan mode, in order to get rid of the spectral response of the optics and detector. As seen in Fig. 2, the TE-polarized PIA spectra reveal a monotonous increase at low energy, which is attributed to free-carrier absorption probably in the ZnO substrate. In turn, the TM-polarized spectra show a sharp resonance. This is indeed expected from the ISB selection rules since only the TM component of the electric polarization couples to the ISB transition. A similar behavior, i.e., the presence of a TM-polarized ISB absorption, is observed for all investigated samples. These resonances are attributed to CB ISB transitions and not to valence band (VB) ISB transitions; the reasons are explained in the Supplemental Material [16].

In order to assess the effect of the corrugation on the confinement energies, we have prepared samples with opposite facets polished at 45° angle to allow infrared light propagation along either the c axis or the a axis. Figure 3 shows the TM- and TE-polarized PIA spectra of sample E at room temperature for the two propagation directions. As seen, the TM-polarized absorption is peaked at 323 (317) meV for light propagating along the c (a) axis. The energy shift is

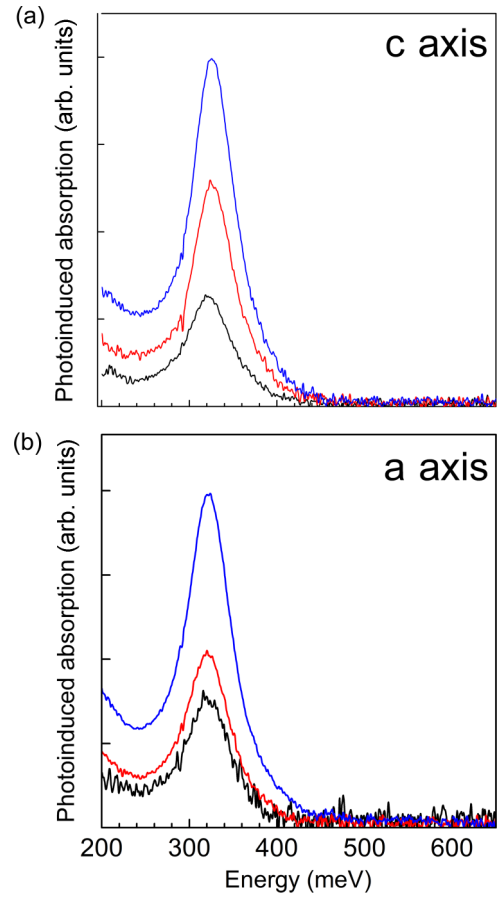

FIG. 3. PIA spectra of sample E at room temperature for TM-polarized light at different UV pump power 40 mW (black), 114 mW (red), and 350 mW (blue) along (a) the c axis and (b) the a axis.

TABLE I. Sample parameters, energy, wavelength, and full width at half maximum (FWHM) of the ISB resonance. The average Mg concentration is deduced from PL measurements. The well and barrier thicknesses are deduced from XRD and APT measurements.

Sample	Mg (%)	Well thickness (nm)	Barrier thickness (nm)	ISB energy (meV)	ISB wavelength (μm)	FWHM (meV)
A	39.5	2.2	15.3	472	2.6	93
B	40.0	2.6	15.0	428	2.9	78
C	39.1	3.1	15.3	362	3.4	64
D	39.9	3.2	15.2	345	3.6	54
E	39.6	3.4	15.2	323	3.8	53
F	39.9	3.8	15.2	300	4.1	52
G	39.6	4.0	14.9	282	4.4	51

only 6 meV which means that the corrugation in the QWs has little effect on the confinement energies, at least at room temperature. In addition, experiments have been carried out by varying the UV pump power from 40 to 350 mW on sample E at room temperature along the *c* and *a* axes, presented in Fig. 3. No measurable change of the TM-polarized ISB resonance peak energy and spectral shape has been observed in this power range, which confirms that the depolarization shift is negligible within our experimental conditions.

Table I summarizes the sample parameters as well as the energy, wavelength, and full width at half maximum (FWHM) of the ISB resonance of all samples. As seen in Table I, the transition energy redshifts with increasing well thicknesses as expected from ISB transitions. The FWHM is around 51 − 54 meV for samples D–F but significantly increases when the well thickness decreases below 3.1 nm. Although one could suspect that for the thinner QWs the excited state gets closer to the continuum leading to the formation of a miniband and resulting in extra broadening, NEXTNANO [15] simulations assuming a CB band offset of 66.5% following Ref. [31] show that the ZnMgO barriers are thick enough to prevent coupling between the QWs, therefore excluding the miniband effect. A more likely explanation is the delocalization of the e_2 envelope function linked to its vicinity to the continuum and the enhanced sensitivity of the ISB transition energy to QW thickness and barrier Mg content fluctuations for the thinner QWs.

IV. RESULTS INTERPRETATION

We have simulated the *bare* ISB transition energy, e_{21}, assuming a Mg concentration in the barrier of 33%, 40%, and 48%, respectively. Figure 4 shows the dependence of the calculated ISB transition energy on the well thickness. It also displays the experimental peak PIA energies. As seen in Fig. 4, the evolution of the experimental PIA transition energy versus well thickness qualitatively follows that of the simulation results. However, the PIA energy exhibits a significant blueshift of the order of 110−115 meV for samples C−G and 125−140 meV for the thinner samples A and B. Further simulations show that this discrepancy cannot be accounted for even by using unrealistic material parameters such as a very high Mg content or a lighter effective mass in ZnO. It should be noted that for previously studied heavily doped samples (i.e., with an electron concentration beyond the Mott transition), the measured PIA ISB transition energy coincided with the ISB energy extracted from standard FTIR spectroscopy; i.e., no blueshift was revealed [5]. This suggests that the observed blueshift of the PIA-measured energies in undoped samples is linked to excitonic effects.

Effectively the binding energy of bulk ZnO excitons is around 60 meV at room temperature and is further enhanced in QW structures due to the quantum electron-hole confinement [25–27]. The binding energy for a 2 nm thick ZnO/ZnMgO QW was estimated to be 115 (87) meV for a

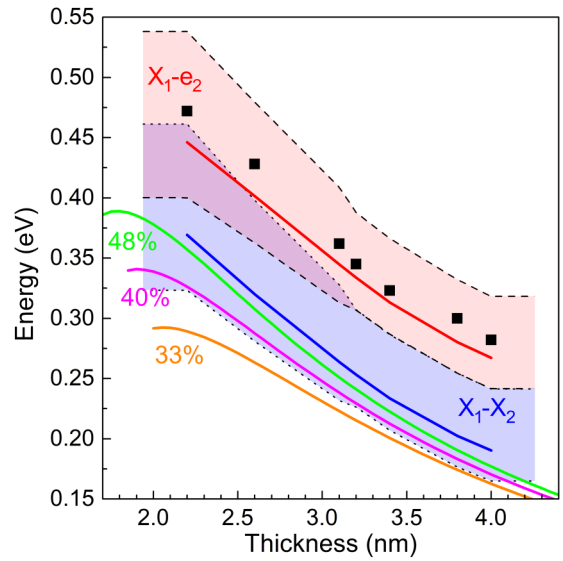

FIG. 4. Calculated CB ISB energy versus well thickness for Mg content in the barrier of 33% (orange curve), 40% (purple curve), and 48% (green curve). The full black squares are the experimental peak energies measured by PIA. The blue curve is the $X_1 - X_2$ (hh_1-e_1 to hh_1-e_2) excitonic transition energy for 40% Mg content, the blue filled area delimited by dots corresponds to the $X_1 - X_2$ transition error accounting for a ± 1 ML fluctuation of the well thickness. The red curve is the ISB energy corrected by the hh_1-e_1 exciton binding energy, which corresponds to a transition X_1-e_2 implying a fundamental excitonic state and an excited e_2 state with unbound electrons and holes and the red filled area delimited by dots corresponds to the X_1-e_2 transition error accounting for a ± 1 ML fluctuation of the well thickness.

TABLE II. Well thickness, and binding energy of the hh_1-e_1 exciton (Δ_1) and of the hh_1-e_2 exciton (Δ_2).

Thickness (nm)	Δ_1 (meV)	Δ_2 (meV)
2.2	108.4	77.0
2.6	104.5	81.6
3.1	99.8	81.1
3.2	98.9	80.7
3.4	97.0	79.8
3.8	93.8	77.8
4	92.4	76.8

Mg content of 27% (12%) [27] in agreement with calculations [26]. For the presently investigated samples, it is estimated to be in the range of $128 - 213$ meV accounting for the actual Mg content. This means that the processes involved in PIA spectroscopy of ZnO heterostructures fundamentally differ from other III–V or IV–IV semiconductors. At room temperature, photoexcited carriers in ZnO QWs are bound by Coulomb interaction and only excitonic interband transitions are present, so the observed PIA transitions are ascribed to the excitonic transition from the X_1 to X_2 $1s$ exciton states, implying the fundamental and first excited excitonic states, induced by the $e_1 - e_2$ ISB absorption. Such effect has already been theoretically predicted by Sadeghi and Li [24].

We have calculated the binding energy of the X_1 to X_2 excitonic transitions with respect to the QW thickness based on Ref. [23] and briefly described in the Supplemental Material [16]. Table II recasts the corresponding values versus well thickness. As expected, the binding energy of the X_1 excitonic transition, Δ_1, increases when the well thickness diminishes [26]. For the X_2 excitonic transition, the binding energy, Δ_2, is smaller than that of the X_1 excitonic transition because of the largest delocalization of the e_2 envelope function with respect to the e_1 envelope function [9,25] and becomes maximum for 2.6 nm thick QWs.

The energy of the transition between $X_1 - X_2$ $1s$ excitonic transition is expressed as $E_{X_1-X_2} = e_{21} + \Delta_1 - \Delta_2$ corresponding to the sum of the $e_1 - e_2$ ISB energy and the difference in the binding energy between the X_1 exciton and the X_2 exciton. This results in a blue shift of the transition energy with respect to the bare ISB energy, as seen in Fig. 4 with the blue curve corresponding to the $X_1 - X_2$ transition. However, the blue-shift is still insufficient to explain the observations. In turn, a good agreement with experiments is achieved when accounting only for the X_1 binding energy correction ($E = e_{21} + \Delta_1$) as observed with the red curve corresponding to the $X_1 - e_2$ transition in Fig. 4. These reported results are different compared to a X_1 to X_2 $1s$ excitonic transition as stated by Olszakier *et al.* [9] and Sadeghi and Li [24]. Our results show that the underlying mechanism for the photoinduced absorption is the dissociation of the X_1 exciton induced by the ISB absorption towards free carriers in the e_2 state, as pictured in Fig. 5. More details involving transition selection rules can be found in the Supplemental Material [16]. Finally, it should be noticed that such ISB induced excitonic effect has never been observed at room temperature in other semiconductor material systems because their exciton binding energy is too small with respect to the thermal energy.

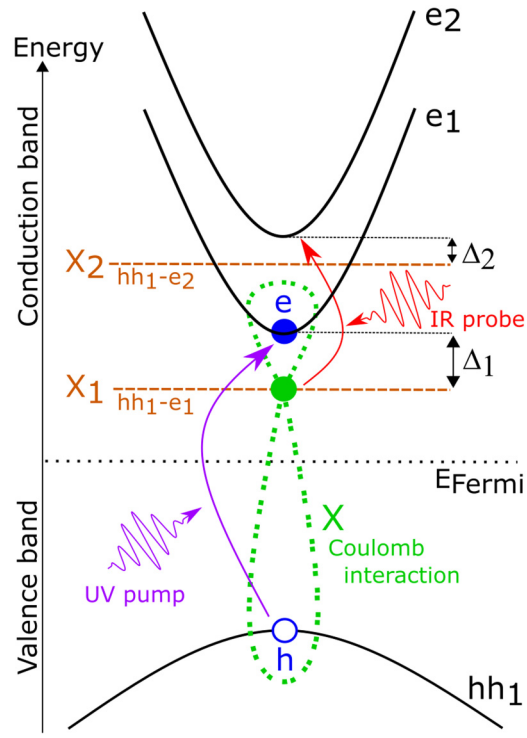

FIG. 5. Scheme of the X_1 (hh_1-e_1) exciton ionization to free carriers in the e_2 state induced by the $e_1 - e_2$ intersubband absorption. The black curved lines represent the electronic states confined in a QW in the conduction and valence bands. The black dotted line is the Fermi energy. The orange dashed lines simulate the excitonic states. The blue full (hollow) dots correspond to electron (hole) particles; their electron-hole Coulomb interaction, symbolized by the green dotted curve, forms an exciton quasiparticle represented by the green dot. The purple (red) arrows illustrate the electron excitation inducing the exciton generation (exciton ionization) by the ultraviolet pump (infrared probe).

V. CONCLUSION

In conclusion, we have performed a systematic study of intersubband absorption of nonintentionally doped m-plane ZnO/ZnMgO QWs using photoinduced infrared absorption spectroscopy under irradiation by a UV laser. All samples exhibit intersubbandlike absorption resonances. However, the peak transition energy is strongly blueshifted with respect to simulations. We claim that the observed transitions, which have never been observed before, involve the dissociation of the hh_1-e_1 exciton induced by the ISB absorption towards unbound electrons in the e_2 state and is supported by the resolution of the X_1 and X_2 exciton binding exciton.

A direct measurement of binding energies could be performed by monitoring the photoluminescence emission dynamics while an UV pump wavelength is tuned from band gap to higher energies [32]. This observation would allow a better understanding of transitions between excitonic states as well

as the development of short-wavelength intersubband devices with near-infrared and even visible operating range. The high binding energies in two-dimensional (2D) materials reaching $\sim$600 meV [33] could be used to explore this phenomenon and unrevealed exotic excitonic transitions.

ACKNOWLEDGMENT

This work was supported by the European Union's Horizon 2020 Research and Innovation FET-Open Program under Grant Agreement No. 665107 (Project ZOTERAC).

[1] M. Belmoubarik, K. Ohtaniand, and H. Ohno, Appl. Phys. Lett. **92**, 191906 (2008).
[2] K. Zhao, G. Chen, B. S. Li, and A. Shen, Appl. Phys. Lett. **104**, 212104 (2014).
[3] E. Belotti, K. Driscoll, T. D. Moustatkas, and R. Paiella, J. Appl. Phys. **105**, 113103 (2009).
[4] S. Kumar, Q. Hu, and J. L. Reno, Appl. Phys. Lett. **94**, 131105 (2009).
[5] N. Le Biavan, M. Hugues, M. Bajo, J. Tamayo-Arriola, A. Jollivet, D. Lefebvre, Y. Cordier, B. Vinter, F. H. Julien, A. Hierro, and J.-M. Chauveau, Appl. Phys. Lett. **111**, 231903 (2017).
[6] M. Montes Bajo, J. Tamayo-Arriola, M. Hugues, J. M. Ulloa, N. Le Biavan, R. Peretti, F. H. Julien, J. Faist, J. M. Chauveau, and A. Hierro, Phys. Rev. Appl. **10**, 024005 (2018).
[7] S. J. Allen, D. C. Tsui, and B. Vinter, Solid State Commun. **20**, 425 (1976).
[8] A. Jollivet, B. Hinkov, S. Pirotta, H. Hoang, S. Derelle, J. Jaeck, M. Tchernycheva, R. Colombelli, A. Bousseksou, M. Hugues, N. Le Biavan, J. Tamayo-Arriola, M. Montes Bajo, L. Rigutti, A. Hierro, G. Strasser, J. M. Chauveau, and F. H. Julien, Appl. Phys. Lett. **113**, 251104 (2018).
[9] M. Olszakier, E. Ehrenfreund, E. Cohen, J. Bajaj, and J. Sullivan, Phys. Rev. Lett. **62**, 2997 (1989).
[10] D. D. Yang, F. H. Julien, J.-M. Lourtioz, P. Boucaud, and R. Planel, IEEE Photon. Technol. Lett. **2**, 398 (1990).
[11] P. Boucaud, L. Gao, Z. Moussa, F. Visocekas, F. H. Julien, J.-M. Lourtioz, I. Sagnes, Y. Campidelli, and P.-A. Badoz, Appl. Phys. Lett. **67**, 2948 (1995).
[12] M. Tchernycheva, L. Nevou, L. Doyennette, F. H. Julien, E. Warde, F. Guillot, E. Monroy, E. Bellet-Amalric, T. Remmele, and M. Albrecht, Phys. Rev. B **73**, 125347 (2006).
[13] S. Sauvage, P. Boucaud, F. H. Julien, J. M. Gerard, and J. Y. Marzin, J. Appl. Phys. **82**, 3396 (1997).
[14] A. Weber, O. Gauthier-Lafaye, F. H. Julien, J. Brault, M. Gendry, Y. Désieres, and T. Benyattou, Appl. Phys. Lett. **74**, 413 (1999).
[15] NEXTNANO3 software, http://www.nextnano.de.
[16] See Supplemental Material at http://link.aps.org/supplemental/10.1103/PhysRevB.105.195143 for a parameters list of the mass-effective model for solving the Schrödinger equation, the investigation of intersubband transitions in the valence band, the calculation procedure of excitonic binding energy, and a study on the influence of the V-groove profile on quantum confinement and its implication on $X_1 - X_2$ interexciton transitions and other transitions.
[17] B. Laumer, F. Schuster, M. Stutzmann, and A. Bergmaier, J. Appl. Phys. **113**, 233512 (2013).
[18] S.-H. Jang and S. F. Chichibu, J. Appl. Phys. **112**, 073503 (2012).
[19] J. Chen, W. Z. Shen, N. B. Chen, D. J. Qui, and H. Z. Wu, J. Phys.: Condens Matter **15**, L475 (2003).
[20] Y.-N. Xu and W. Y. Ching, Phys. Rev. B **43**, 4461 (1991).
[21] T. C. Damen, S. P. S. Porto, and B. Tell, Phys. Rev. **142**, 570 (1966).
[22] A. R. Denton and N. W. Ashcroft, Phys. Rev. A **43**, 3161 (1991).
[23] R. P. Leavitt and J. W. Little, Phys. Rev. B **42**, 11774 (1990).
[24] S. M. Sadeghi and W. Li, IEEE J. Quantum Electron. **40**, 343 (2004).
[25] D. G. Thomas, J. Phys. Chem. Solids **15**, 86 (1960).
[26] G. Bastard, J. A. Brum, and R. Ferreira, J. Appl. Phys. **72**, 3218 (1992).
[27] G. Coli and K. K. Bajaj, Appl. Phys. Lett. **78**, 2861 (2001).
[28] H. D. Sun, T. Makino, Y. Segawa, M. Kawasaki, A. Ohtomo, K. Tamura, and H. Koinuma, J. Appl. Phys. **91**, 1993 (2002).
[29] H. Matsui, N. Hasuike, H. Harima, and H. Tabata, J. Appl. Phys. **104**, 094309 (2008).
[30] E. Di Russo, J. Houard, S. Moldovan, G. Da Costa, I. Blum, F. H. Julien, M. Tchernycheva, J. M. Chauveau, M. Hugues, D. Blavette, and L. Rigutti, Appl. Phys. Lett. **111**, 032108 (2017).
[31] H. Yin, J. Chen, Y. Wang, J. Wang, and H. Guo, Sci. Rep. **7**, 41567 (2017).
[32] A. Tzimis, A. V. Trifonov, G. Christmann, S. I. Tsintzos, Z. Hatzopoulos, I. V. Ignatiev, A. V. Kavokin, and P. G. Savvidis, Appl. Phys. Lett. **107**, 101101 (2015).
[33] T. Mueller and E. Malic, 2D Mater Appl. **2**, 29 (2018).